JOURNAL OF COMPUTATIONAL PHYSICS 121, 129–141 (1995)

An Investigation of Some Pattern Selection Issues in the Rising Plane Taylor Bubble Problem

PRABIR DARIPA

Department of Mathematics, Texas A&M University, College Station, Texas 77843

Received November 17, 1993; revised December 23, 1994

Plane Taylor bubbles with correct and incorrect tip angles are numerically generated for the case of zero surface tension (s.t.) using a Fourier collocation method. We find that all of these bubbles satisfy correct asymptotic shape at their tails. We have identified some generic patterns in the behavior of these bubbles with incorrect tip angles. We provide theoretical justifications of these observations and provide some validation criteria for solutions with correct tip angle. We derive a tip angle dependent higher order constraint on the solution at the tip and show this to be a very useful validation criterion. The usefulness of this criterion is exemplified by allowing tip angles of bubbles to be determined numerically. The relevance of our results to accurate computation of the nature of selection mechanism for the zero s.t. limit bubble is discussed.

1. INTRODUCTION

A plane bubble rising in a tube models the late stages of Rayleigh–Taylor instability, i.e., instability of a planar interface separating a heavy fluid from a light fluid when a force is pointing from the heavy to the light fluid. We consider a symmetric bubble rising at a constant velocity U in a two-dimensional channel of width h (see Fig. 1). The interior angle at the tip of the bubble is denoted by θ_t. The flow exterior to the bubble is considered inviscid and incompressible. In the absence of surface tension (s.t.) T, this problem is characterized by two parameters, θ_t and F, where

$$F = U/\sqrt{gh}. \tag{1}$$

Here g is the gravitational acceleration and the Froude number, F, refers to the dimensionless speed of the bubble. The principal issues have been the determination of allowable values of F and θ_t and of the asymptotic shape of the tail of the bubble interface (i.e., for large x downstream; see Fig. 1). Theoretically, it can be shown that allowable values of θ_t are 180°, 120°, and 0° (see Section 3) and the asymptotic shape of the bubble interface for large x downstream is

$$x = -F^2/2(1 - 2y)^2. \tag{2}$$

The asymptotic shape (2) serves to partially validate numerical calculations. Determination of allowable values of F has been analytically intractable. Birkhoff [1, 2] and Birkhoff and Carter [3] were first to formulate this problem in the absence of surface tension. They also addressed various issues related to this problem and the problem of laminar mixing. Based on their formulation and calculations, Birkhoff and Carter predicted the speed of the zero s.t. smooth bubble somewhere between 0.21 and 0.24. However, Garabedian [8] predicted the nonuniqueness of these zero s.t. smooth bubbles rising at any $F \leq 0.24$. Recent numerical calculation of Vanden-Broeck [19] shows the following: smooth bubbles for $F < F_c$, cusped bubbles for $F > F_c$ and pointed bubbles with $\theta_t = 120°$ for $F = F_c$, where $F_c = 0.35775$. Thus, there is a general agreement about the existence of a continuum of zero s.t. smooth bubbles.

However, bubbles which have been observed experimentally [6, 7, 12, 14] (two- and three-dimensional) in the presence of surface tension have unique s.t. dependent speeds, even when s.t. is negligibly small. When s.t. is negligibly small, two-dimensional bubbles of Lewis [12] rise at a speed which is slightly higher than theoretical estimates of Garabedian and Birkhoff based on zero surface tension. Birkhoff [1] explains the possible cause of such discrepancies between theoretical and experimental data. However, there seems to be a general consensus that the idealized two-dimensional bubble in the limit of zero s.t. should have speed somewhere between 0.23 and 0.24. The selection of such a unique zero s.t. limit bubble out of a continuum of zero s.t. smooth bubbles was subsequently explained by the numerical results of Vanden-Broeck [18].

There have been later calculations on this problem in the presence of s.t. by other investigators including Couët and Strumolo [4] and Kessler and Levine [10]. The general agreement among these investigators is that there is a discrete set of smooth bubbles embedded in a continuum of pointed bubbles. However, there are discrepancies between the calculations of Vanden-Broeck [18] and Couët and Strumolo [4] on the zero s.t. limit behavior of the smooth bubbles. Vanden-Broeck [18] finds that zero s.t. limit of all smooth non-zero s.t. bubbles is a unique bubble with $F \sim 0.23$. However, Couët and Strumolo [4] using the same method as in [18] finds that

0021-9991/95 $12.00

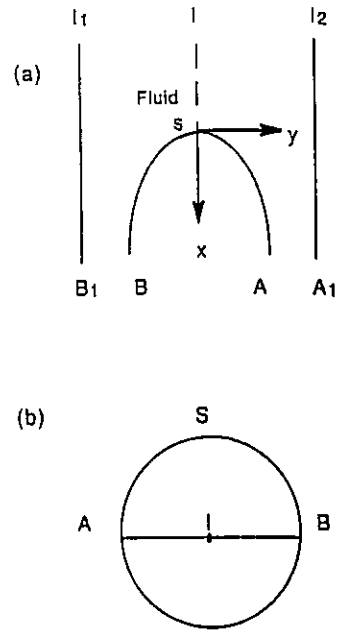

FIG. 1. (a) The physical region: a bubble is rising upward in the fluid with speed U. The diameter of the tube is h. (b) The circle plane: $|\sigma| \leq 1$.

the least upper bound of the sequence of Froude numbers of the non-zero s.t. smooth bubbles is approximately 0.23 as $T \to 0$. Thus degeneracy is not removed in the zero s.t. limit according to Couët and Strumolo [4]. We speculate that the disagreement between this limit behavior results of Vanden-Broeck and Couët and Strumolo may lie in misinterpretation of the numerical results since their calculation procedures are identical.

The issue that concerns us here is the discrepancy between the calculation of Kessler and Levine [10] and later calculation of Vanden-Broeck [20] on the quantitative estimates of the selection mechanism. Kessler and Levine [10] uses a numerical procedure based on the representation of the solution in integral form using appropriate Green's function for the problem. These investigators characterize the selection mechanism quantitatively by the rate of approach of the pointed bubbles to the smooth bubbles in the limit of zero surface tension. To be precise, these investigators estimate numerically $(\theta_t/\pi - 1)$ as a function of T as $T \to 0$. Vanden-Broeck [18] finds that $(\theta_t/\pi - 1)$ is exponentially small in T, whereas Kessler and Levine [10] finds that their "mismatch function" which is the same as $(\theta_t/\pi - 1)$ is algebraically small in T. It is worth pointing out that the selection mechanism of such solitary patterns in the contexts of crystal growth and Saffman–Taylor finger is known to be associated with exponentially small terms in T. In these related problems, exact known zero s.t. solutions are used in the explanation of selection mechanism by analyses of asymptotics beyond all orders [11]. However, such exact analyses have not been possible for the bubble problem due to the lack of exact known zero s.t. solutions which are starting points in these analyses. Therefore the question of precise nature of selection mechanism for this problem remains open and it remains to be seen whether selection mechanism is exponential or algebraic.

The above disagreement between the calculations of Kessler and Levine [10] and Vanden-Broeck [18] may be due to the difficulty in computing correct values of tip angles of these non-zero s.t. pointed bubbles. These bubbles, even if physically meaningless, need to be computed correctly in order to resolve the above discrepancy in the selection mechanism. We must state right away that we do not resolve this issue here. Instead, we argue that one of the possible causes of the above disagreement is that the previous validation studies on these non-zero s.t. pointed bubbles may not have been strict enough. Our argument is based on consideration of this problem without s.t., where we have a priori knowledge of correct values of the tip angles of mathematically admissible bubbles. This allows us to test the possibility of generating pointed bubbles with incorrect tip angles. In particular, we show that numerical solutions with seemingly incorrect tip angles seem to converge to solutions with correct shape at the tail. We derive a tip angle dependent new higher order constraint on the solution at the tip and call this validation criterion as "tip selection criterion" (TSC in short). We show that construction of numerical solutions using TSC, in particular where the tip angle is determined numerically, is important because it indicates that numerical solution reflects the properties of the continuous problem and has the correct tip angle. We also identify some generic patterns in the behavior of these bubbles with incorrect tip angles. We provide theoretical justifications of these observations and some validation criteria for solutions with correct tip angles. The usefulness of these criteria in numerical determination of tip angle is shown by allowing tip angles of bubbles to be determined numerically. The relevance of our results to accurate computation of the nature of the selection mechanism for the zero s.t. limit bubble is also discussed. Hope is that our analyses and numerical results presented here will shed some light on the difficulty in numerically resolving the issue of the selection mechanism without stricter validation criteria.

The rest of the paper is laid out as follows. In Section 2, mathematical formulation of this problem is given for the sake of completeness and for our future reference. In Section 3 we provide a new higher order constraint on the solution at the tip and use it to prove that the bubbles are either round, cusped, or pointed with 120° angle at the tip. We discuss a numerical method in Section 4 and present numerical results in Section 5. In Section 6, we provide some theory which explains most of our numerical observations. In Section 7, we list some validation criteria and suggest ways to improve the numerical method for the purpose of remedying such spurious solutions with incorrect tip angles. We finally conclude in Section 8.

2. PRELIMINARIES

The plane potential flow past a symmetric and infinitely long bubble (see Fig. 1), $y = f(x)$, rising in a tube of width h at a speed U, is usually formulated in a frame of reference attached to the bubble. With respect to the reference frame attached to the bubble, the fluid upstream has a speed U downward. Henceforth all variables will be appropriately normalized, speed by U and time by (h/U). Since the fluid is incompressible, flow can be described in terms of a potential ϕ and a stream function ψ.

The potential plane image of Fig. 1 is the infinite strip $0 \le \psi \le 1$; the slit $\psi = \frac{1}{2}$, $\phi > 0$ is the image of the interface; and the lines $\psi = 0$, $\psi = 1$ are the walls of the tube. The complex potential $w = \phi + i\psi$ is an analytic function of the complex variable $z = x + iy$ due to incompressibility of the flow field. In the potential plane, the problem reduces to constructing the complex velocity $\tau = \ln q - i\theta = \nu - i\theta$ as an analytic function of w within the strip shown in the potential plane. Here q is the speed and θ is the flow direction. The following system then describes the flow in the potential plane:

$$\tau = \tau(w) \quad \text{in } 0 < \psi < 1, -\infty \le \phi \le \infty, \tag{3a}$$

$$q^2 - \frac{2}{F^2}x = \text{const}, \quad \text{on } \psi = \frac{1}{2}, \phi > 0, \tag{3b}$$

$$\theta = 0, q = 1 \quad \text{as } \phi \to -\infty, 0 \le \psi \le 1, \tag{3c}$$

$$\theta = 0 \quad \text{on } \psi = 0, \psi = 1, -\infty < \phi < \infty. \tag{3d}$$

The solution $\tau(w)$ of the system (3) is used to integrate the equation

$$\frac{dz}{dw} = q^{-1}e^{i\theta} = e^{-\tau(w)}, \tag{4}$$

on $w = \phi + i/2$, $\phi \ge 0$, to generate the bubble surface. It is convenient to work in terms of an auxiliary complex variable σ which is introduced by the conformal mapping

$$e^{-\pi w} = \tfrac{1}{2}(\sigma^{-1} - \sigma). \tag{5}$$

This mapping maps the bubble surface onto upper semi-circle $\sigma = e^{i\alpha}$; $\alpha \in [0, \pi]$, the walls on the real axis and the flow domain onto the interior of the domain bounded by the upper semi-circle and the real axis (see Fig. 1b). The bubble surface is obtained from integrating

$$z_\alpha = z_\phi \phi_\alpha = -\frac{\cot \alpha}{\pi q} e^{i\theta}, \quad 0 \le \alpha \le \pi, \tag{6}$$

which is obtained from (4) and (5). The values of $q(\alpha)$ and $\theta(\alpha)$ on the unit semi-circle are obtained by solving the following system which is the analog of system (3) in the circle plane,

$$\tau = \tau(\sigma) \quad \text{in } |\sigma| \le 1, 0 \le \alpha \le \pi, \tag{7a}$$

$$qq_\alpha - \frac{1}{F^2}x_\alpha = 0 \quad \text{on } \sigma = e^{i\alpha}, 0 \le \alpha \le \pi, \tag{7b}$$

$$\tau(0) = 0, \tag{7c}$$

$$\text{Imag}(\tau(\sigma = r)) = 0, \quad -1 \le r \le 1, \alpha = 0. \tag{7d}$$

The interface condition (7b) is obtained by differentiating (3b) on the unit semi-circle. Here and below a subscript denotes differentiation with respect to that variable. In addition, $\tau(\sigma)$ should satisfy the following conditions due to symmetry requirement of the bubble surface,

$$\tau(\sigma) = \bar{\tau}(-\bar{\sigma}), \tag{8}$$

where an overbar denotes complex conjugacy. Due to (7d), $\tau(\sigma)$ can be continued analytically across the real line in the domain bounded by the lower semi-circle and the real axis. Thus by Schwartz reflection principle we have

$$\tau(\sigma) = \bar{\tau}(\bar{\sigma}) \quad \text{in } |\sigma| \le 1. \tag{9}$$

The asymptotic behaviors of τ at the tail ($\sigma = \mp 1$) and at the tip ($\sigma = i$) of the bubbles are given by

$$\begin{aligned} e^\tau &\approx [-\ln C(1 - \sigma^2)]^{1/3} \\ &\text{as } \sigma \to \mp 1; \quad e^\tau \approx (1 + \sigma^2)^\gamma \quad \text{as } \sigma \to i, \end{aligned} \tag{10}$$

where $\gamma = \theta_t/\pi \ge 0$ with θ_t as the included angle of the bubble at the tip. An appropriate representation of $\tau(\sigma)$ in $|\sigma| \le 1$ satisfying (7a) and (7c) through (9) is given by

$$\begin{aligned} e^{\tau(\sigma)} = (1 + \sigma^2)^\gamma [-\ln C(1 - \sigma^2)]^{1/3} [-\ln C]^{-1/3} \\ \exp\left(\sum_{n=1}^{\infty} a_n \sigma^{2n}\right), \end{aligned} \tag{11}$$

and using (4), the boundary condition (7b) can be rewritten for the symmetric half of the bubble as

$$\pi \tan \alpha e^{2\nu} \frac{d\nu}{d\alpha} + \frac{e^{-\nu}}{F^2} \cos \theta = 0, \quad 0 \le \alpha \le \frac{\pi}{2}. \tag{12}$$

In (11) the Fourier coefficients, a_n, are real and $0 < C < 0.5$. The values of ν and θ, obtained from solving (12) subject to (11), determine the shape of the bubble form (6).

Equation (12) is a nonlinear eigenvalue problem with two parameters F and γ (γ appears because of harmonic conjugacy of ν and θ according to (11)). The admissible values of F so that (12) has solutions have been computed numerically [10, 19]. The allowable values of the other parameter, γ, are known to be 0, $\frac{2}{3}$, and 1 on heuristic ground (see Garabedian [9] and

Modi [13]). In the next section, we give a new derivation for the admissible values of γ.

3. SELECTION OF THE TIP ANGLE AND A NECESSARY CONDITION FOR THE ADMISSIBILITY OF NUMERICAL SOLUTIONS

The flow field in the exterior of the bubble is governed by Laplace's equation which, in theory, would allow any arbitrary angle at the tip of the bubble if it were not for the boundary condition (12). Therefore, selection of the tip angle must be hidden in the boundary condition. Without the use of this condition, one can at most infer from (10) that $q = O(\beta^\gamma)$ as $\beta = \pi/2 - \alpha \to 0$, suggesting that $q_c = q|_{\beta=0}$ is zero unless the tip of the bubble is a cusp ($\gamma = 0$). Here $\beta = 0$ corresponds to the tip of the bubble. As seen below, a trivial manipulation of the boundary condition (12) reveals the allowable values of the tip angle, the local behavior of q at the tip of the bubble, and a relation which is computationally useful. The boundary condition (12) can be rewritten as

$$\frac{d}{d\beta}(q^3) = \frac{3}{\pi F^2}\tan\beta\cos\theta, \quad 0 \le \beta < \frac{\pi}{2}, \tag{13}$$

which is true for any arbitrary value of the tip angle θ_t. It then follows that the following must hold at the tip ($\beta = 0$) of the bubbles,

$$(q^3)_{\beta|\beta=0} = 0; \quad \frac{\pi F^2}{3}(q^3)_{\beta\beta|\beta=0} = \cos(\theta_t/2). \tag{14b}$$

(Note that $(q^3)_{\beta\beta|\beta=0}$ is zero for a round bubble which follows from (14b), as well as from (10).) The allowable form of q in powers of β which is consistent with (14) as $\beta \to 0$ is

$$q = q_c + \left(\frac{3}{2\pi F^2}\cos(\theta_t/2)\right)^{1/3}\beta^{2/3} + O(\beta^\lambda); \quad \lambda > \tfrac{2}{3}. \tag{15}$$

For pointed bubbles ($0 < \theta_t < \pi$), the leading power of β in (15) is $\frac{2}{3}$ which implies that allowable pointed bubbles must have $\theta_t = 120°$. Also, note that cusped bubbles are possible corresponding to $q_c \neq 0$ in (15). Round bubbles are possible since the second term in (15) then vanishes and q must then be $O(\beta)$. This concludes the rederivation of the allowable values of the tip angle. Below we use the notation θ_a to denote any one of these allowable values of tip angle.

The computational relevance of our result in this section is obvious. Equation (14b) can be used as a necessary condition for the admissibility of numerical solutions, in addition to Eq. (2). This will provide added confidence in the numerical results. It should be noted that both of these results are asymptotic results: Eq. (2) at the tail and Eq. (14b) at the tip. As we will see the local result (14b) is useful computationally. Below we refer to Eq. (14b) as TSC, an abbreviated form for tip selection criterion.

4. A NUMERICAL METHOD

The expressions for ν, θ and their derivatives from (11) are substituted into (12). This gives an equation containing F, θ_t, and an infinite number of Fourier coefficients a_n. In order to solve it numerically, only a finite number of Fourier coefficients are retained and this equation is applied at N equi-spaced points: $\alpha_I = (\pi/2N)(I - \frac{1}{2})$, $I = 1, \ldots, N$. This gives a system of N nonlinear equations which is solved by Newton's iterations for N unknowns. Numerical convergence in Newton's iterations for any choice of N is achieved if the values of the unknowns do not change more than 10^{-8} between two successive Newton iterations. The computations were performed on a Cray-YMP in single precision. Once this is solved, values of q and θ at mesh points are obtained from (11) and the bubble is obtained by integrating (6). Numerical solutions are obtained in this fashion for a sequence of values of $N \le 501$. Unless otherwise mentioned or exemplified, our results will correspond to cases where, with increasing N, the tail end of the Fourier spectrum tends to zero and the power series in (11) at the collocation points appears to converge from our studies with $N \le 501$. The values of N unknowns and the shapes of the bubble profiles corresponding to these values of N are tested for convergence. Numerical results of the next section fall into two categories, depending on the choices of N unknowns: (i) N Fourier coefficients (F and θ_t prescribed); and (ii) $N - 1$ Fourier coefficients and θ_t (F prescribed).

Two important remarks should be made regarding this numerical method. First, the mesh points are deliberately selected in a way to avoid the end-point singularities (see Eq. (10)): the real part of τ (i.e., $\nu = \log q$) in (12) is unbounded at such end-point singularities. Second, numerical procedure requires evaluating ν, θ, and $d\nu/d\alpha$ (see Eq. (12)) at the mesh points and no higher order derivatives. This makes the finite resolution calculations of this method somewhat insensitive to important higher order effects such as the TSC, i.e., (14b).

5. NUMERICAL RESULTS

Among many case studies that we have done, only some case studies are presented below. We summarize these numerical results as follows:

(a) Numerical solutions in which $\theta_t = \theta_a$. One case from this category corresponding to $F = 0.23$, $\theta_t = 180°$, referred below as case (i), is presented.

(b) Numerical solutions in which $\theta_t \neq \theta_a$. In particular, we discuss solutions in which θ_t is close to θ_a versus solutions in which θ_t is not close to θ_a. Two cases for each of these subcategories are discussed. Thus there are four cases from this category. From the first subcategory, results presented correspond

to $F = 0.23$, $\theta_t = 178°$ (referred to below as case (ii)) and $F = 0.35775$, $\theta_t = 118°$ (referred to below as case (iii)). It helps to keep in mind there is a general consensus that Eqs. (11) and (12) have solutions when $F = 0.23$, $\theta_t = 180°$ and also when $F \sim 0.35775$, $\theta_t = 120°$. From the second subcategory, results presented correspond to $F = 0.40$, $\theta_t = 90°$ (referred to below as case (iv)) and $F = 0.35$, $\theta_t = 135°$ (referred to below as case (v)). Here again it helps to keep in mind that there is numerical evidence that Eqs. (11) and (12) admit solutions when ($F = 0.40$, $\theta_t = 0°$) and ($F \sim 0.35$, $\theta_t = 180°$).

(c) Numerical solutions in which the parameter θ_t in (11) is determined numerically by treating it as a free parameter in the numerical procedure. Results of many case studies in this category are presented in a concise manner.

There are altogether five cases from the categories (a) and (b) in the above list. We find that interfaces generated with N up to 251 (in some cases we have used N up to $N = 501$) converge in most cases to seemingly smooth profiles away from the tip which satisfy the correct theoretical shape at the tail. Case (i) corresponds to the correct parameter values and thus needs no further explanation. For cases (ii) through (iv) (results under category (b) above), it helps first to show the bubble profiles in Fig. 2 and Fig. 3. Figure 2a shows numerically generated bubble profiles for cases (ii) and (iii) when $N = 121$. These bubble profiles seem to converge (Fig. 2(c) and Fig. 2(d)) and to agree well with the correct asymptotics at the tail (Fig. 2(b)). Similarly, Fig. 3(a) shows numerically generated bubble profiles for cases (iii) and (v) when $N = 121$. Except in a small neighborhood near the tip for case (iv) (see Fig. 3(d)) these bubble profiles seem to converge (Fig. 3(c) and Fig. 3(d)) and to agree well with the correct asymptotics at the tail (Fig. 3(b)).

Next we show numerical results mentioned under category (c) above in which the parameter θ_t in (11) is determined numerically by treating it as a free parameter in the numerical procedure. In all of these calculations, $\theta_t = 180°$ is used as initial guess for the tip angle. Figure 4(a) shows rates of convergence of tip angles in Newton's iterations (see Section 4) for values of $F \leq 0.29$ when $N = 121$. Figure 4(b) shows converged values of θ_t against F for different choices of N. Convergence of the plots, θ_t vs. F, to the correct one, i.e., $\theta_t = 180°$, is seen to be very slow. All bubbles with $F > 0.15$ in our calculations of Fig. 4 at $N = 121$ satisfy the correct asymptotic shape at the tail of the bubble. For $F < 0.15$, a larger number of collocation points would be required so that the corresponding bubbles satisfy the correct asymptotic shape at the tail of the bubble. There is a consistent theoretical explanation as to why these bubbles under categories (b) and (c) above with $\theta_t \neq \theta_a$ satisfy the correct asymptotic (2) at the tail. We defer this explanation until the next section.

Since we want to give theoretical justification of some of our numerical observations, we find it helpful to subdivide these observations into following five categories.

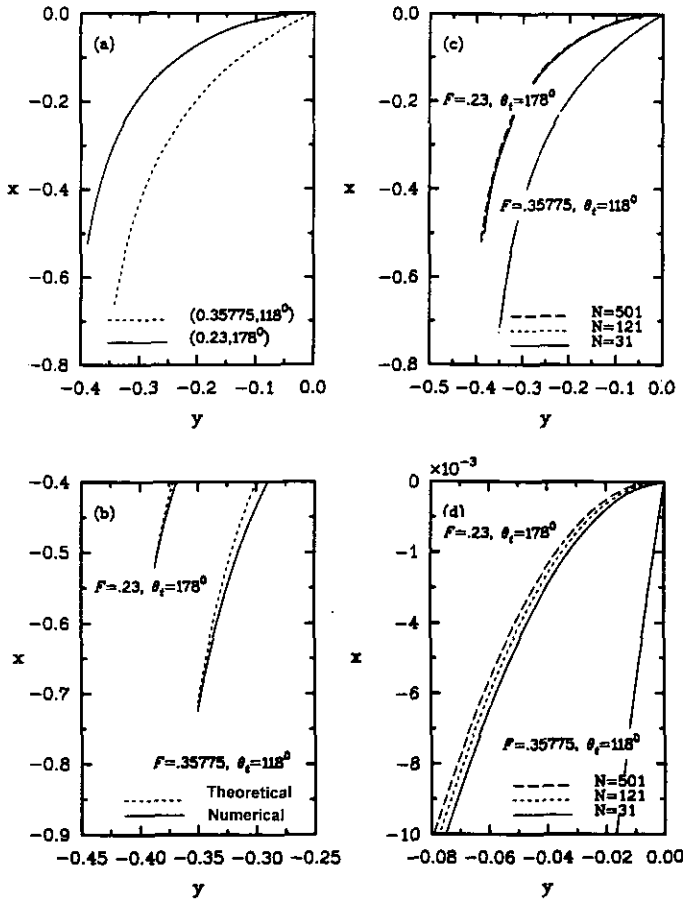

FIG. 2. Numerically induced spurious bubbles: (a) bubble profiles with $F = 0.35775$, $\theta_t = 118°$ (left branch) and $F = 0.23$, $\theta_t = 178°$ (right branch), $N = 121$; (b) comparison of theoretical and numerical shapes of tails of the bubbles, $N = 121$; (c) convergence of bubble profiles; (d) magnified view of shapes of bubble profiles near the tip for various values of N (note the scales of the figure).

5.1. *List of Observations.* (i) Tip selection criterion (TSC). There are altogether five cases from the categories (a) and (b) in the list of calculations mentioned in the beginning of Section 5. Table I shows numerical and theoretical values of the TSC for these five cases.

The decimal places up to which numerical and theoretical values of the TSC agree deteriorate from the second for case (i) (the correct solution where $(\theta_t - \theta_a) = 0$) to the one for cases (ii) and (iii) ($(\theta_t - \theta_a) = 0$) to none for cases (iv) and (v), where $(\theta_t - \theta_a)$ is not small. Similar results about the value of TSC is borne out by calculations leading to Fig. 4, where θ_t is determined numerically. Corresponding values of TSC are shown in Fig. 5. Figure 5 shows left (Fig. 5(a)) and right (Fig. 5(b)) hand sides of the TSC (see Eq. (14(b)) against F for runs where θ_t is determined numerically as discussed under category (c) above. As we see from Figs. 4 and 5, $\theta_t \sim \theta_a = 180°$ for these runs and agreement between theoretical and numerical

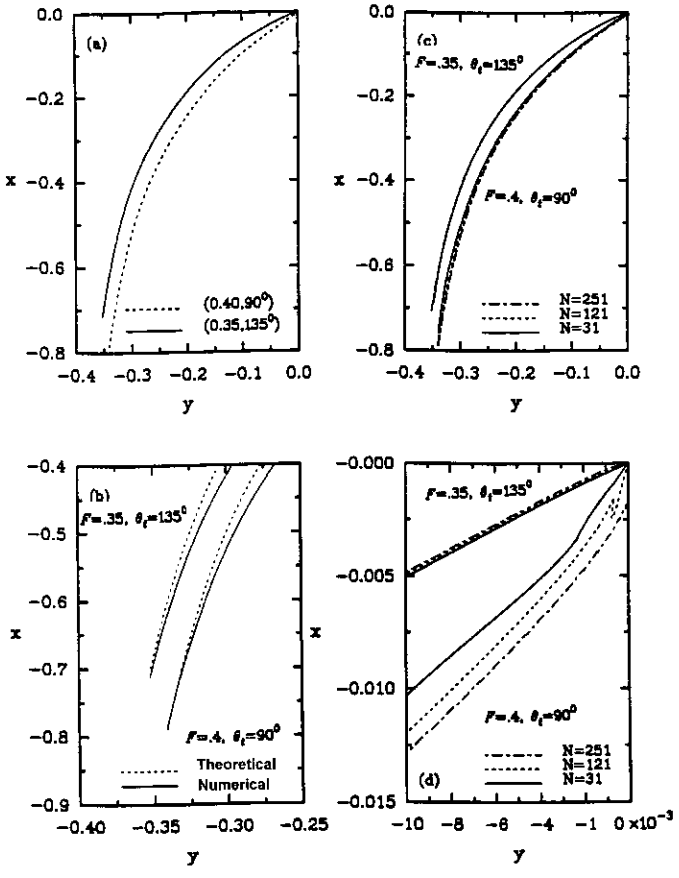

FIG. 3. Numerically induced spurious bubbles: (a) bubble profiles with $F = 0.40$, $\theta_t = 90°$ (left branch) and $F = 0.35$, $\theta_t = 135°$ (right branch), $N = 121$; (b) comparison of theoretical and numerical shapes of tails of the bubbles, $N = 121$; (c) convergence of bubble profiles; (d) magnified view of shapes of bubble profiles near the tip for various values of N (note scales of the figure).

values of TSC are up to two decimal places similar to the cases (ii) and (iii) of Table I. In summary, TSC seems to be a useful validation criterion for the tip angle.

(ii) Asymptotic behavior of the Fourier coefficients. Table II shows the frequency of oscillations in the Fourier coefficients for the cases in Table I and Fig. 6 shows the same for cases corresponding to Fig. 4, where θ_t is determined numerically.

Table II and Fig. 6 show that there are oscillations in the Fourier coefficients for all solutions with $\theta_t \neq \theta_a$. In particular, we find that the values of the Fourier coefficients for these solutions alternate in sign asymptotically, regardless of the number of collocation points used in our calculations with $N \geq 31$. As such, oscillations in the Fourier coefficients are acceptable for correct solutions also, even though there are no oscillations in the Fourier spectrum for case (i). Since such oscillations in some cases are too small to be visible within the resolution of the plots of a_n vs. n, we plot $\log_{10} a_n$ vs. n when $N = 251$ for cases (i) through (v) of Table I in Fig. 7. From these and many other runs not reported here we find that Fourier coefficients of numerical solutions with $\theta_t \neq \theta_a$ alternate in sign asymptotically. We see that for $n \sim N$, $|a_n| \leq 10^{-4}$ for the first three cases and $|a_n| \leq 10^{-3}$ for the last two cases. For the last case (v), amplitude of the Fourier coefficients a_n do not seem to decrease after some n (see Fig. 7(e)). Nonetheless, bubbles generated with these Fourier coefficients seem to have smooth profiles as we have shown in Fig. 3. In Fig. 8 we show plots of $\ln n$ vs. n for these cases. Figure 8(a) shows the algebraic decay rate of the Fourier coefficients for the correct solution with $F = 0.23$, $\theta_t = 180°$. We find that $a_n = O(n^{-1.3})$ in this case.

In summary, we find that perturbation of the parameter θ_t about θ_a (cases (i) and (ii) in Table II) will cause the Fourier coefficients of the numerical solutions to alternate in sign asymptotically. Theoretical explanation of this is given in the next section.

(iii) Behavior of the Fourier series. The Fourier series (see Eq. (11)) seem to converge from our calculations at all collocation points. We also investigated the behavior of this series at

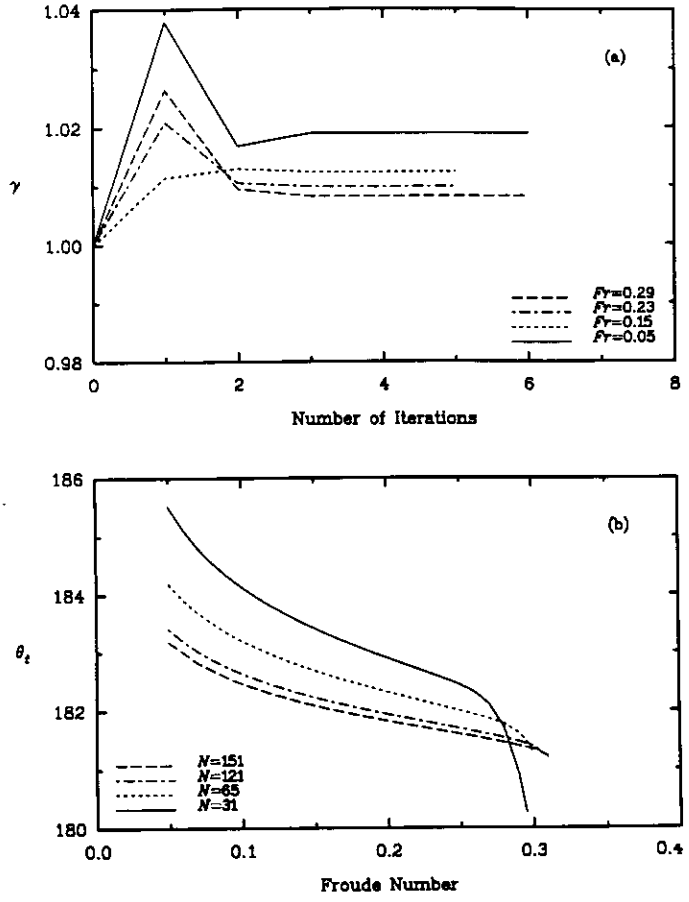

FIG. 4. Convergence of the tip angle: (a) convergence of γ with number of iterations for various values of Froude number with $N = 121$. (b) converged values of the tip angle, θ_t, as a function of Froude number for various values of N.

TABLE I

Theoretical and Numerical Values of $(\pi F^2/3)(q^3)_{\beta\beta}|_{\beta=0}$

Case	(F, θ_t)	$N = 31$	$N = 121$	$N = 251$	$N = 501$	Theoretical
i	(0.23, 180°)	0.001385	0.001385	0.001385	0.001385	0.0
ii	(0.23, 178°)	0.00143	0.00138	0.00135	0.00135	0.0174
iii	(0.35775, 118°)	0.488	0.466	0.462	0.460	0.515
iv	(0.40, 90°)	15.31	69.73	18.14	—	0.7071068
v	(0.35, 135°)	0.236	0.146	0.136	0.164	0.3826834

the tip which is not one of the collocation points. If we denote the sum of the first N terms of the Fourier series at the tip by S_N, then the sequence $\{S_{31}, S_{121}, S_{251}\}$ for the five cases in Table I are respectively $\{-0.02986, -0.02519, -0.02947\}$, $\{-0.07465, -0.08939, -0.09790\}$, $\{-0.11329, -0.13346, -0.15589\}$, $\{0.26178, 0.08929, 1.25812\}$, and $\{0.10223, 0.03062, -0.06904\}$. Note that there is no indication of any divergence of these sequences for any of these cases. We will show in the next section, the sum S_N should diverge at the tip for $\theta_t \neq \theta_a$ and the lack of any indication of this divergence in the series from the above sequence is due to slow divergence of the series at the tip.

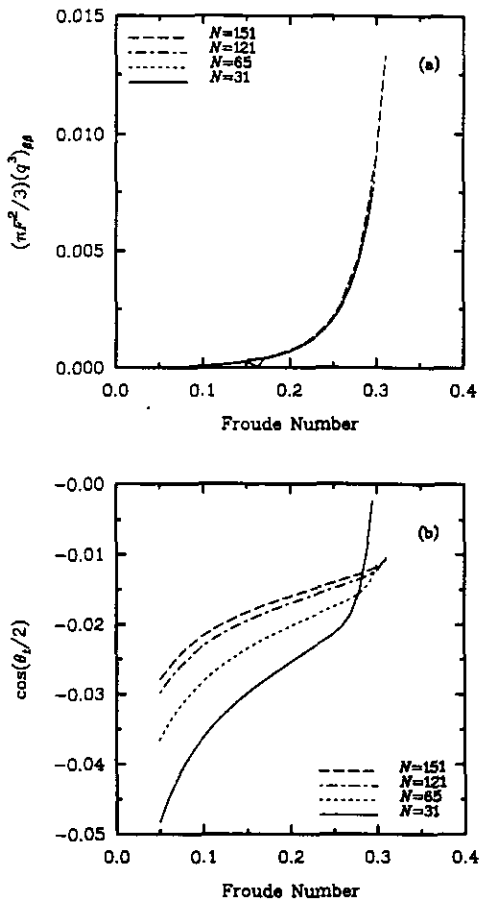

FIG. 5. Tip selection criterion: $\cos(\theta_t/2) = (\pi F^2)/3(q^3)_{\beta\beta}$ at the tip: (a) $(\pi F^2/3)(q^3)_{\beta\beta}$ vs F at the tip of the bubbles. (b) $\cos(\theta_t/2)$ vs F.

(iv) Behavior of θ near the tip: It is useful to recall that $\lim_{\beta\to 0} \theta(\beta)$ is the flow direction on the bubble interface as the tip $\beta = 0$ (see Section 3 for a definition of β) is approached from the left side of the interface (see Fig. 1). Therefore, this limit should be equal to $-(\theta_t/2)$ for a correct value of θ_t. In Fig. 9 through 13 we show q and θ against β. Figure 9(c) through 13(c) respectively show magnified views of the plots 9(b) through 13(b) near the tip of the bubble. Note that in each of these cases the flow direction θ near the tip seems to be approaching a value close to its correct value as the tip is approached. This is particularly remarkable for the case (iv) (see Table I), where we have $\theta \sim 0$ near the tip even though we have used $\theta_t = 90°$ ($\theta = 0$ is the correct tip angle in this case). Moreover, we see that θ vs. β plots oscillate near the tip of bubble for the cases (ii) through (iv). All of these, including the oscillations in Fig. 9(c) through 13(c), are explained in Section 5.

(v) Numerical determination of θ_t: Fig. 4(b) shows that error in θ_t is small, of the order of 2° to 3° when $N = 251$ since the correct value of $\theta_t(F)$ is 180° for values of F in this figure. Error is small because our initial guess is the correct value 180° (see Fig. 4(a)). For an initial guess far from the correct value, the error can be large or small, depending on the initial guesses of the Fourier coefficients also. In summary, the numerically obtained value of θ_t for a given F need not be the correct tip angle. There is a logical explanation as to why θ_t in our numeri-

TABLE II

Percentage of Oscillations in the Fourier Coefficients

Case	(F, θ_t)	$N = 31$	$N = 121$	$N = 251$	$N = 501$
i	(0.23, 180°)	0.0	0.0	0.0	0.0
ii	(0.23, 178°)	86.2	96.6	98.4	99.2
iii	(0.35775, 118°)	93.1	98.32	99.2	100
iv	(0.40, 90°)	89.6	97.5	98.8	100
v	(0.35, 135°)	93.1	99.1	99.6	100

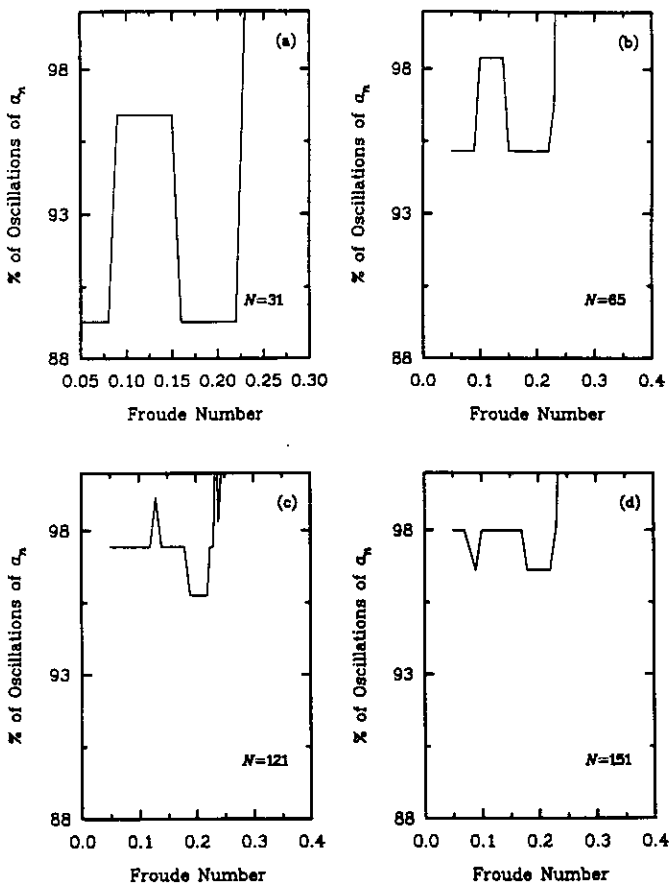

FIG. 6. Percentage of oscillations of Fourier coefficients as a function of Froude number for various values of N. In these calculations, the tip angle is treated as a free parameter.

cal procedure may converge to a value not necessarily close to the correct tip angle. This is explained in Section 6.

(vi) Asymptotic shape at the tail: Finally we should also list here our observation that most of these numerical solutions with $\theta_t \neq \theta_a$ seem to converge to bubbles with the correct asymptotic shape (2) at the tail.

The above subdivision reflects the way in which the following section is organized.

6. DISCUSSIONS

We first provide theoretical justification of the numerical observations listed in the previous section. It is convenient first to write the logarithm of Eq. (11) in the form

$$\tilde{\tau}(\sigma; \theta_t) = g(\sigma; \theta_t), \quad |\sigma| \leq 1, \tag{16}$$

where we have used

$$\tilde{\tau}(\sigma; \theta_t) = \tau(\sigma) - \frac{\theta_t}{\pi}\ln(1 + \sigma^2) + h(C, \sigma) \tag{17}$$

and

$$g(\sigma; \theta_t) = \sum_{n=1}^{\infty} a_n(\theta_t)\sigma^{2n}. \tag{18}$$

The exact form of $h(C, \sigma)$ which can be deduced from (11) and (17) is not important here. It suffices to note that $h(C, \sigma)$ does not depend either on θ_t or on F and its value is real at the tip $\sigma = i$. In (18), we have explicitly emphasized dependency of the Fourier coefficients, a_n, on the parameter, θ_t, which facilitates our discussion below. Theoretical explanations of the observations listed in 5.1 are given below in the same order as in 5.1.

(i) Tip selection criterion (TSC). TSC, i.e., Eq. (14b), depends on θ_t and the selection mechanism of the tip angles θ_a is hidden in this. Therefore, numerical solutions with $\theta_t \neq \theta_a$ do not satisfy the TSC.

(ii) Asymptotic behavior of the Fourier coefficients. Use of correct tip angle θ_a for θ_t in (17) makes $\tilde{\tau}(\sigma; \theta_t)$ bounded and continuous. Therefore, the series $g(\sigma; \theta_a)$ for $\tilde{\tau}(\sigma; \theta_a)$ (see Eq. (16)) will converge pointwise to $\tilde{\tau}(\sigma; \theta_a)$ at all points on

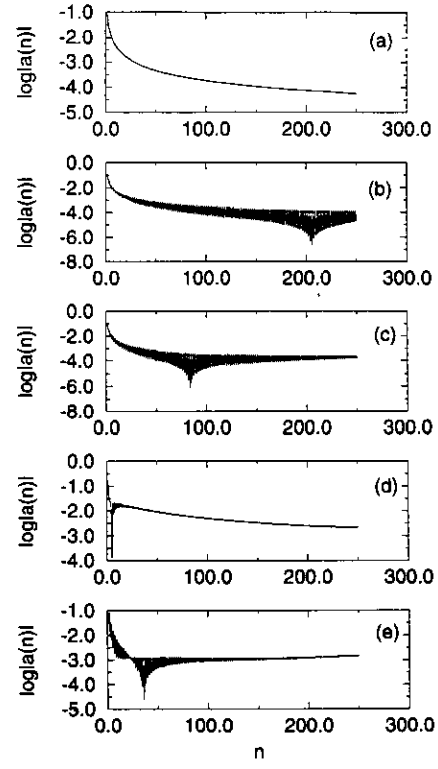

FIG. 7. Plot of $\log_{10}|a_n|$ vs n for the five cases in Table I when $N = 251$: (a) $F = 0.23$, $\theta_t = 180°$; (b) $F = 0.23$, $\theta_t = 178°$; (c) $F = 0.35775$, $\theta_t = 118°$; (d) $F = 0.40$, $\theta_t = 90°$; (e) $F = 0.35$, $\theta_t = 135°$.

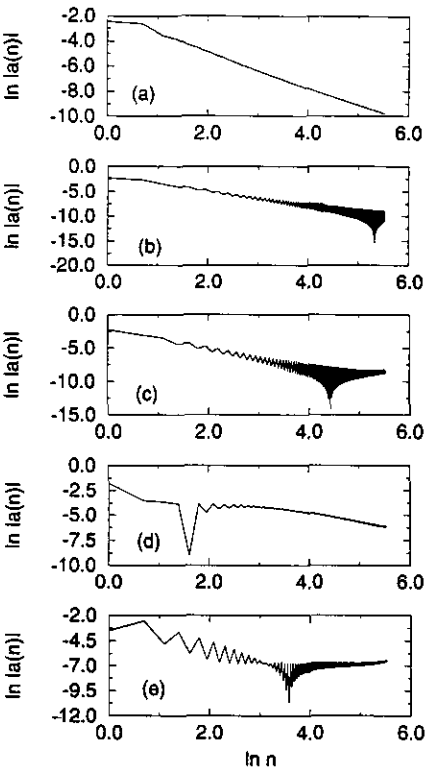

FIG. 8. Plot of $\ln|a_n|$ vs $\ln n$ for the five cases in Table I when $N = 251$: (a) $F = 0.23$, $\theta_t = 180°$. The plot is linear for large n with slope $= -1.3$, suggesting that $a_n = O(n^{-1.3})$ for $n \to \infty$; (b) $F = 0.23$, $\theta_t = 178°$; (c) $F = 0.35775$, $\theta_t = 118°$; (d) $F = 0.40$, $\theta_t = 90°$; (e) $F = 0.35$, $\theta_t = 135°$.

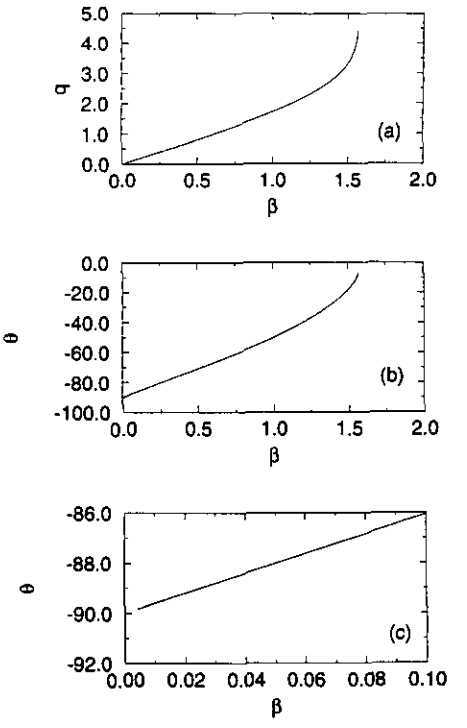

FIG. 9. Plots of speed (q) and flow direction (θ) when $N = 251$, $F = 0.23$, $\theta_t = 180°$ (case (i) in Table I). $\beta = 0$ is the tip and $\beta = \pi$ is the tail of the bubble: (a) q vs β; (b) θ vs β; (c) blow-up of figure (b) near the tip.

the unit circle. From the continuity of $\bar{\tau}(\sigma;\ \theta_a)$ on the unit circle, it follows that $a_n(\theta_a) = O(1/n)$ as $n \to \infty$, i.e., $\lim_{n\to\infty} |a_n/n| < \infty$ (see [15]). This estimate is most conservative and in reality the Fourier coefficients are found to decay faster than this from our numerical calculations. For example, for the case (i) in Table I we find that $a_n = O(n^{-1.3})$ as $n \to \infty$ (see 5.1 and also Fig. 8(a)). Therefore, it will be fair for our purposes to assume that

$$a_n(\theta_a) = o(1/n) \quad \text{as } n \to \infty. \tag{19}$$

On the other hand, use of $\theta_t \neq \theta_a$ in (17) introduces a logarithmic singularity in $\bar{\tau}(\sigma;\ \theta_t)$ at $\sigma = i$ and therefore the series $g(\sigma;\ \theta_t)$ in (18) will converge everywhere except at the tip.

It is convenient to rewrite (17) in the form

$$\bar{\tau}(\sigma;\ \theta_t) = \bar{\tau}(\sigma;\ \theta_a) + \varepsilon \ln(1 + \sigma^2), \quad |\sigma| \leq 1, \tag{20}$$

where $\varepsilon = (\theta_a - \theta_t)/\pi$ is a measure of deviation of θ_t from θ_a. The Taylor series expansion for $\ln(1 + \sigma^2)$ about $\sigma = 0$ is given by

$$\ln(1 + \sigma^2) = \sum_{n=1}^{\infty} \frac{(-1)^{n+1}}{n} \sigma^{2n}, \tag{21}$$

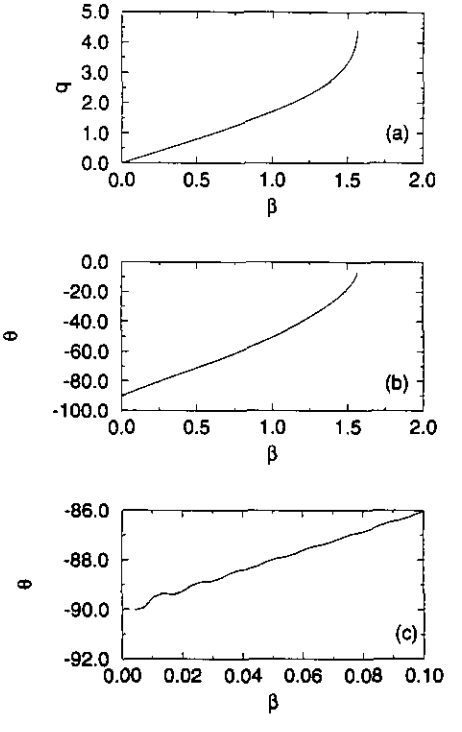

FIG. 10. Plots of speed (q) and flow direction (θ) when $N = 251$, $F = 0.23$, $\theta_t = 178°$ (case (ii) in Table I). $\beta = 0$ is the tip and $\beta = \pi$ is the tail of the bubble: (a) q vs β; (b) θ vs β; (c) blow-up of figure (b) near the tip.

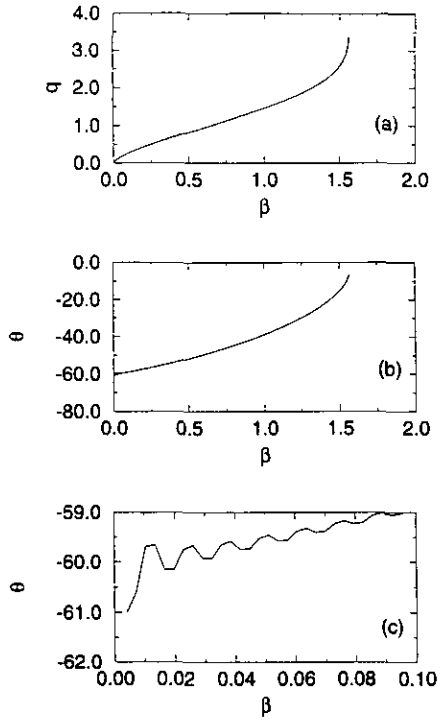

FIG. 11. Plots of speed (q) and flow direction (θ) when $N = 251$, $F = 0.35775$, $\theta_t = 118°$ (case (iii) in Table I). $\beta = 0$ is the tip and $\beta = \pi$ is the tail of the bubble: (a) q vs β; (b) θ_t vs β; (c) blow-up of figure (b) near the tip.

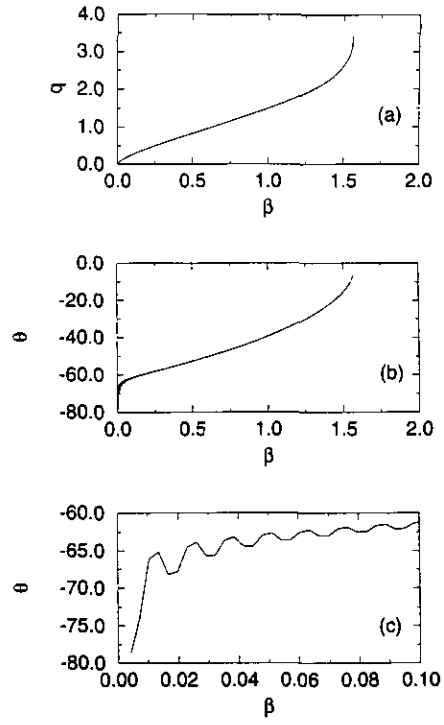

FIG. 13. Plots of speed (q) and flow direction (θ) when $N = 251$, $F = 0.35$, $\theta_t = 135°$ (case (v) in Table I). $\beta = 0$ is the tip and $\beta = \pi$ is the tail of the bubble: (a) q vs β; (b) θ_t vs β; (c) blow-up of figure (b) near the tip.

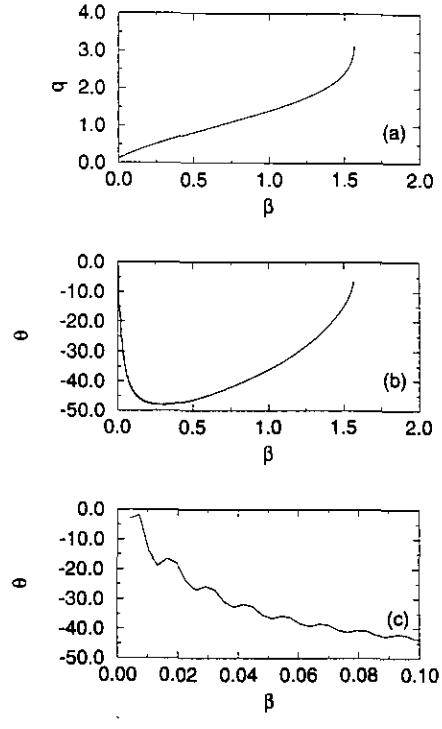

FIG. 12. Plots of speed (q) and flow direction (θ) when $N = 251$, $F = 0.40$, $\theta_t = 90°$ (case (iv) in Table I). $\beta = 0$ is the tip and $\beta = \pi$ is the tail of the bubble: (a) q vs β; (b) θ_t vs β; (c) blow-up of figure (b) near the tip.

which coverges for $|\sigma| \leq 1$, except at $\sigma = \mp i$ ($\sigma = i$ represents the tip of the bubble). Therefore, Eqs. (20) and (21) imply that the Taylor series $g(\sigma; \theta_t)$ for $\tilde{\tau}(\sigma; \theta_t)$ with $\theta_t \neq \theta_a$, will converge for $|\sigma| \leq 1$, except at $\sigma = \mp i$. Substituting the series (18) for $\tilde{\tau}$ and the series (21) for $\ln(1 + \sigma^2)$ in (20) and equating like powers in σ, which is legitimate for points away from the tip, we obtain

$$a_n(\theta_t) = a_n(\theta_a) + \varepsilon \frac{(-1)^{n+1}}{n}, \quad n \geq 1. \tag{22}$$

From (19) and (22), it then follows that for $\theta_t \neq \theta_a$,

$$a_n(\theta_t) \sim \varepsilon \frac{(-1)^{n+1}}{n} \quad \text{as } n \to \infty. \tag{23}$$

This explains the oscillations in the Fourier coefficients as $n \to \infty$ tabulated in Table II and seen in Figs. 6, 7, and 8.

(iii) Behavior of the Fourier series at and near the tip. The origin of some of the observations including oscillations in the bubble interface near the tip in Fig. 3(d) can be traced in the term $\varepsilon \ln(1 + \sigma^2)$ in Eq. (20). On the bubble interface $\sigma = e^{i\alpha}$, this logarithmic term which has a branch point at $\sigma = i$ becomes

$$\varepsilon \ln(1 + e^{2i\alpha}) = \varepsilon \ln|2 \cos \alpha| + i\varepsilon S(\alpha), \tag{24}$$

where the discontinuous function $S(\alpha)$ is given by

$$S(\alpha) = \begin{cases} \alpha, & 0 < \alpha < \pi/2 \\ \alpha - \pi, & \pi/2 < \alpha < 3\pi/2 \\ \alpha - 2\pi, & 3\pi/2 < \alpha < 2\pi. \end{cases} \tag{25}$$

From (21) and (24) we have for $\alpha \neq \pi/2, 3\pi/2$,

$$\ln|2 \cos \alpha| = \sum_{n=1}^{\infty} \frac{(-1)^{n+1}}{n} \cos 2n\alpha,$$
$$S(\alpha) = \sum_{n=1}^{\infty} \frac{(-1)^{n+1}}{n} \sin 2n\alpha. \tag{26}$$

The Fourier series for $\ln|2 \cos \alpha|$ converges everywhere to the function, except at the tip. At the tip, the function diverges logarithmically, whereas the series diverges as $-\sum_{n=1}^{\infty} (1/n)$. Note that these divergence rates are slow and about the same. This causes the Fourier series of Eq. (11) to diverge very slowly at the tip which may not be that easily evident from numerical calculation with a modest number of collocation points. This explains our observation (iii) in 5.1.

(iv) Behavior of θ near the tip. According to Eq. (20), flow direction θ, the imaginary part of τ, depends on the imaginary part of $\varepsilon \ln(1 + e^{2i\alpha})$, i.e., $\varepsilon S(\alpha)$, and therefore the computed values of θ near the tip will behave the same way as the convergence properties of $\varepsilon S(\alpha)$. The Fourier series for the discontinuous function $S(\alpha)$ defined in (25) converges with the familiar Gibb's phenomenon (see page 149 in [15]) in the neighborhood of the tip; i.e., the series converges to the function $S(\alpha)$ with oscillations near the tip. This explains the oscillations in θ near the tip when $\theta_t \neq \theta_a$.

Our discussion and derivation of Eq. (17) suggests that the solution $\tau(\sigma)$ at a specific F away from the tip is not affected by the choice of θ_t because any changes in the right-hand side of (17) due to nonzero $\theta_t - \theta_a$ is exactly balanced by appropriate changes in the Fourier coefficients, a_n, which determine the left-hand side of (17) through (18). It helps to recall that the Fourier coefficients depend on θ_t through (22), regardless of whether θ_t is equal to θ_a or not. This explains why the flow direction near the tip is close to its correct value regardless of the value of θ_t.

(v) Numerical determination of θ_t. We observed that the numerically determined value of θ_t need not be the correct tip angle θ_a. The explanation lies in Eq. (17) which suggests that for a correct solution $\tau(\sigma)$ of (11) and (12), there are infinitely many choices of θ_t, because to each choice of θ_t there is a unique set of Fourier coefficients given by (22) and, hence, a unique $\tilde{\tau}$ given by (18). The values to which the unknowns θ_t and the Fourier coefficients $\{a_n(\theta_t)\}$ converge depend on the initial guesses for these unknowns and all sets of converged values refer to the same legitimate solution with correct tip angle θ_a. This explains the results of our calculations leading to Fig. 4. The converged values in Fig. 4(b) are close to the correct tip angle, 180°, because the initial guess in all these calculations is taken to be the correct tip angle as seen in Fig. 4(a).

(vi) Aysmptotic shape at the tail. Numerical solutions with $\theta_t \neq \theta_a$ satisfy the correct asymptotic shape (2) at the tail because of two reasons: (i) it does not depend on θ_t; and (ii) the numerical solution $\tau(\sigma)$ converges to the correct solution away from the tip. Therefore, the bubble shape obtained from integrating (4) should be the correct one corresponding to the correct value of θ_a. The oscillations in the bubble shape such as in Fig. 3 for the case (iv) have to do with the effect of the finite grid size because the convergence of the Fourier series for θ is not uniform and suffers from Gibb's phenomenon near the tip. In cases (ii) through (iv), we do not see these oscillations within the resolution of the plots because in these cases the integration of Eq. (4), used in obtaining these bubble interfaces, provides very good smoothing of these oscillations in θ.

Finally, we should address the problem of the possibility of estimating θ_a from calculations with $\theta_t \neq \theta_a$. Since the choice of the parameter θ_t should not affect the solution $\tau(\sigma)$ and the bubble shape away from the tip, it may seem viable to obtain a good estimate of θ_a from the computed flow direction near the tip of the bubble. From practical considerations, however, this estimate may not be good enough in all cases as justified below.

6.1. *Theoretical Estimate of θ_a when $\theta_t \neq \theta_a$.* It is convenient to introduce the variable θ_c through

$$\theta_c = -2 \lim_{\alpha \to \pi/2} \theta(\alpha). \tag{27}$$

Note that $\lim_{\alpha \to \pi/2} \theta(\alpha)$ is the flow direction on the bubble interface as the tip is approached from the left side of the bubble (see Fig. 1) and therefore θ_c is referred to here as the computed value of the tip angle. Below we give a theoretical estimate of θ_a in terms of θ_t and θ_c. From our analysis above it should be obvious that all these angles assume the same value when θ_t is the correct tip angle.

To establish a relationship between these three angles when $\theta_t \neq \theta_a$, we should first recall from standard Fourier series analysis of the sawtooth function $S(\alpha)$ (see [15]) that the series for $S(\alpha)$ for $\alpha \to \pi/2$ will be approximately 9% higher than $\lim_{\alpha \to \pi/2} S(\alpha)$ due to Gibb's phenomenon, i.e.,

$$\lim_{\alpha \to \pi/2} \left(\sum_{n=1}^{\infty} \frac{(-1)^{n+1}}{n} \sin 2n\alpha \right) \sim 1.09 \lim_{\alpha \to \pi/2} S(\alpha) = 1.09 \frac{\pi}{2}. \tag{28}$$

Keeping in mind that $\tau = \ln q - i\theta$, the imaginary part of (16) on the bubble interface away from the tip is

$$-\theta(\alpha) - \frac{\theta_t}{\pi} S(\alpha) + \text{Imag}(h(C, \sigma = e^{i\alpha})) = \sum_{n=1}^{\infty} a_n(\theta_t)\sin 2n\alpha. \tag{29}$$

For $\theta_t = \theta_a$, use of (25) and the fact that $h(\cdot)$ is real at the tip renders the left-hand side of this equation zero and continuous at the tip and, therefore, we have

$$\lim_{\alpha \to \pi/2} \left(\sum_{n=1}^{\infty} a_n(\theta_a)\sin 2n\alpha \right) = 0. \tag{30}$$

For $\theta_t \neq \theta_a$, we have from (29),

$$-\lim_{\alpha \to \pi/2} \theta(\alpha) - \frac{\theta_t}{2} = \varepsilon \lim_{\alpha \to \pi/2} \left(\sum_{n=1}^{\infty} \frac{(-1)^{n+1}}{n} \sin 2n\alpha \right), \tag{31}$$

where we have made use of (22), (30, (25), and the fact that $h(\cdot)$ is real at the tip. From (28) and (31) we then have

$$-\lim_{\alpha \to \pi/2} \theta(\alpha) - \frac{\theta_t}{2} \sim 1.09 \left(\frac{\theta_a - \theta_t}{2} \right), \tag{32}$$

where we have used $\varepsilon = (\theta_a - \theta_t)/\pi$. In terms of θ_c (see Eq. (27)), Eq. (32) then becomes

$$(\theta_c - \theta_t) \sim 1.09(\theta_a - \theta_t), \tag{33}$$

or, alternatively, we have

$$(\theta_c - \theta_a) \sim 0.09(\theta_a - \theta_t), \tag{34}$$

which gives the correct tip angle θ_a in terms of θ_t and θ_c. Below we estimate θ_a using (27) and (34) and denote this estimated value by θ_a^c. It should be emphasized that θ_a is one of the three correct angles, whereas θ_a^c is the approximate value of any one of these angle numerically estimated by the above procedure.

In principle, the computed value of θ at the collocation point nearest to the tip can be extrapolated to obtain the limiting value $\lim_{\alpha \to \pi/2} \theta(\alpha)$ which can then be used in (27) to obtain an approximate estimate of θ_c. This value of θ_c and known θ_t then can be used in (34) to obtain θ_a^c. To see the merit of this method, we calculated θ_a^c for the cases tabulated in Table I by the above procedure and compared with the known values of θ_a. The θ_a^c and θ_a for these five cases are respectively (180°, 180°), (180.09°, 180°), (122.62°, 120°), (15.5°, 0.0), and (173.07°, 180°). The estimates of θ_a^c for the last three cases are not good, but it is really quite remarkable that these estimates are not worse. These results could have been worse because there is a fundamental difficulty in obtaining a good estimate of θ_c from finite resolution calculations. To see this, note from (27) that estimating θ_c requires evaluating the limit in the right-hand side of (27) from the series in (29). The series in (29) converges nonuniformly away from the tip for $\theta_t \neq \theta_a$ due to the asymptotic behavior (23) of the Fourier coefficients in (29) (i.e., due to Gibb's phenomenon). This can cause some error in the estimated value of the limit in the right-hand side of (27) from its value at the collocation point nearest to the tip of the bubble by any ad hoc extrapolation (we have used linear extrapolation in the above calculation). Besides, convergence of the series in (29) deteriorates considerably due to slow decay rate of the Fourier coefficients (see (23)). This should also be evident from the plots in Fig. 7 and 8.

The function $\theta_a^c(F)$ undoubtably depends sensitively on the value of θ_a^c at each F. Even a small error in the estimate of θ_a at each F can cause the function $\theta_a^c(F)$ to deviate significantly from the desired function $\theta_a(F)$. Similarly, the numerically determined function $\theta_t(F)$ can deviate significantly from the desired function $\theta_a(F)$ since the numerically determined value of θ_t at any F need not be the corresponding θ_a for reasons discussed earlier. For example, consider the numerical results resulting in Fig. 4(b). If we take the plot of θ_t vs. F when $N = 151$ as a good approximation to the desired function $\theta_a(F)$, then we see in Fig. 4(b) that $\theta_t(F)$ is a polynomial of some degree higher than one. On the other hand, we know that the desired function $\theta_a(F)$ is a polynomial of degree zero ($\theta_a(F) = 180°$). Thus, there is some inherent difficulty in numerically predicting the correct functional form of the desired function $\theta_a(F)$ from numerically determined values of θ_t or θ_c at various F. We believe that this should be true even when the surface tension is nonzero. We conjecture that the difficulty in obtaining a reliable estimate of the selection mechanism would be similar. Even though we have not addressed the problem here with nonzero surface tension, our hope is that these results will shed some light on this problem, in particular, possible sources of disagreement among various investigators about the estimate of selection mechanism in the presence of surface tension.

7. VALIDATION CRITERIA AND REMEDIAL OF SPURIOUS SOLUTIONS

The effect of using $\theta_t \neq \theta_a$ is explained and exemplified in the previous sections. However, all of these effects arising due to $\theta_t \neq \theta_a$ are not suitable for validation purposes because some of these do not necessarily imply that $\theta_t \neq \theta_a$. For example, oscillations in the Fourier spectrum are prefectly acceptable for legitimate solutions. However, we can clearly identify the following implementable criteria for validation of numerical solutions other than the asymptotics (2) at the tail.

(i) Tip selection criterion (TSC). The tip selection criterion, i.e., Eq. (14(b)), will not be satisfied for $\theta_t \neq \theta_a$. This criteria is useful because it can be used a priori or a posteriori. A priori use of this as an auxilary equation in our numerical procedure will guarantee that θ_t is the correct tip angle of the numerical solutions.

We incorporated TSC in the numerical method to remedy numerical solutions for $\theta_t \neq \theta_a$. We made the following modifications of the method described in Section 4: (i) truncate the Fourier series after $(N + 1)$ terms instead of N terms; and (ii) increase the number of equations from N to $N + 1$ by using Eq. (14(b)) at $\alpha = \pi/2$ after substituting appropriate expressions for q and θ and their derivatives from truncated version of (11) into (14(b)). We tested this strategy and were not able to obtain any solutions for $\theta_t \neq \theta_a$ and thus we were successful in remedying the spurious solutions. However, we should point out that this modification of the method deteriorates the convergence properties of the Newton iterations when $\theta_t = \theta_a$. This is not very surprising because the TSC imposes a constraint on the allowable values of the Fourier coefficients.

(ii) Behavior of θ near the tip. If θ_c, given by (27), equals θ_t, then θ_t is the correct tip angle θ_a according to (33). This, of course, assumes that we have a good estimate of θ_c from our computations. This can be estimated from numerical results in the same way as we have done in the previous section. Also, as noted earlier, $\theta(\alpha)$ should converge uniformly for correct solutions everywhere. Usually for $\theta_t \neq \theta_a$, the convergence will not be uniform and $\theta(\alpha)$ will oscillate near the tip.

8. CONCLUSIONS

We have derived a new higher order constraint on the solution at the tip of zero s.t. bubbles. We have exemplified its usefulness in detecting spurious solutions and shown this to be a stricter validation criterion than the asymptotics at the tail. We have also explained the difficulty in accurate evaluation of tip angles numerically and suggested some validation criteria for tip angles. We have emphasized that this can cause significant error in the numerical determination of the function describing the dependency of the tip angle on the speed (F) of the bubbles. We have argued that the difficulties could be similar in the presence of surface tension and could be the source of disagreement among various investigators about the selection mechanism of the zero s.t. limit bubble. We have emphasized the need for improved convergence and validation studies to resolve this disagreement.

ACKNOWLEDGMENTS

I thank one of the referees for helpful suggestions. This research has been supported in part by NSF Grants DMS-8803669 and DMS-9208061. It has also been supported by NASA under Contract NAS1-19480. The allocation of computer resources by the Texas A&M Supercomputer Center and NASA Langley Research Center is gratefully acknowledged.

REFERENCES

1. G. Birkhoff, Los Alamos Report LA-1862, pp. 1–76, 1954 (unpublished).
2. G. Birkhoff, Los Alamos Report LA-1927, pp. 1–91, 1956 (unpublished).
3. G. Birkhoff and D. Carter, *J. Math. Phys.* **6,** 769 (1957).
4. B. Couët and G. S. Strumolo, *J. Fluid. Mech.* **184,** 1 (1987).
5. P. Daripa, *J. Comput. Phys.* **88,** 337 (1990).
6. R. M. Davies and G. I. Taylor, *Proc. R. Soc. London Ser A* **200,** 375 (1950).
7. D. T. Dumitrescu, *Z. Angew. Math. Mech.* **23,** 139 (1943).
8. P. R. Garabedian, *Proc. R. Soc. London Ser. A* **241,** 423 (1957).
9. P. R. Garabedian, *Commun. Pure Appl. Math.* **38,** 609 (1985).
10. D. A. Kessler, and H. Levine, *Phys. Rev. A* **39,** 5462 (1989).
11. M. D. Kruskal, and H. Segur, *Stud. Appl. Math.* **85,** 129 (1991).
12. D. J. Lewis, *Proc. R. Soc. London Ser. A* **202,** 81 (1950).
13. V. Modi, *Phys. Fluids* **28,** 3432 (1985).
14. D. J. Nicklin, J. O. Wilkes, and J. F. Davidson, *Trans. Inst. Chem. Eng.* **40,** 61 (1962).
15. L. Sirovich, *Introduction to Applied Mathematics* (Springer-Verlag, New York/Berlin, 1988).
16. C. Sulem, P. L. Sulem, and H. Frisch, *J. Comput. Phys.* **50,** 138 (1983).
17. G. I. Taylor, *Proc. R. Soc. London Ser. A* **201,** 192 (1950).
18. J.-M. Vanden-Broeck, *Phys. Fluids* **27,** 2604 (1984).
19. J.-M. Vanden-Broeck, *Phys. Fluids* **29,** 1343 (1986).
20. J.-M. Vanden-Broeck, *Phys. Fluids* **4,** 2332 (1992).